Effects of carbon nanotube (CNT) geometries on the dispersion characterizations and adhesion properties of CNT reinforced epoxy composites

Dawei Zhang [a], Ying Huang [a]* and Leonard Chia [a]

[a] *Department of Civil and Environmental Engineering, North Dakota State University, USA 58108*

**Corresponding author: Associate Professor, North Dakota State University, CIE201F, 1340 Administration Ave., Fargo, ND 58108, USA, Email:* ying.huang@ndsu.edu*;*

Phone: 701-231-7651; ORCID number: 0000-0003-4119-9522

Abstract

Carbon nanotubes (CNTs) are widely added into polymeric materials as additives to improve the mechanical properties of the composites. The great variances of CNTs in geometries including different diameters and lengths may inevitably result in extensive differences on material properties and reinforcing efficiencies in CNT reinforced epoxy composites. This paper investigated the dispersion characterizations and adhesion properties of CNT reinforced epoxy composites with different CNT geometries including three different CNT diameters and two different lengths by particle size analysis, single lap shear (SLS) tests, transmission and scanning electron microscopy (TEM and SEM). The experimental results showed that CNTs with larger diameter (50-100 nm) had a greater ability to achieve more uniform dispersion which further led to better adhesion properties. Although CNT length did not have an evident effect on the CNT dispersion, epoxy composites reinforced by normal-length CNTs (5-20 μm) had higher lap shear strength and toughness than those by shorter CNTs (0.5-2 μm).

Keywords: Carbon nanotube (CNT), epoxy composites, CNT geometries, particle size analysis, single lap shear test, electron microscopy

1. Introduction

Carbon nanotube (CNT) is generally recognized as a one-dimensional material with extremely high aspect ratio, specific strength, and stiffness [1]. These outstanding mechanical properties along with notable thermal and electrical conductivities have motivated various applications of CNTs in a wide range of fields and industries [2,3]. The CNTs have great potential of introducing advanced properties into polymers by forming CNT reinforced composites [4–6], even compared to other nano fillers [7, 8]. One of the ideal polymeric materials containing CNTs as nanofillers is epoxy resin, which has excellent corrosion resistance and chemical stability [9]. In civil and transportation engineering, CNT reinforced epoxy composites can be used to bond similar and dissimilar materials in the form of adhesive joints or to be applied on the surface of steel structures as anti-corrosive coatings [10–13]. Most of the usages of CNT reinforced epoxy composites require a solid adhesive bonding between the epoxy composite and the substrate material, since a weak adhesion may easily lead to the early failure of adhesive joints or the debonding of protective coatings, which makes adhesion properties of crucial importance to the overall performance of CNT reinforced epoxy composites.

Shear or bonding strength is the governing parameter of adhesion properties, while single lap shear (SLS) tests were exclusively used to determine the lap shear strength of polymeric matrices on metal substrates [14–16]. A number of researches has been incorporating CNTs into epoxy resin and trying to improve the lap shear strength or adhesion properties of CNT reinforced epoxy composites. However, inconsistency with

46 their findings were noticed. Some studies showed that the lap shear strength of CNT
47 reinforced epoxy composites was significantly higher than that of neat epoxy composite,
48 with the improvement as high as 39% [17, 18]. While, it is found by some other studies
49 that the improvements of lap shear strength were relatively limited with the similar surface
50 conditions, similar epoxy components, and same weight fraction of CNTs (around 0.5%).
51 Compared to neat epoxy composites, only slightly increases in lap shear strength (typically
52 less than 10%) were reported with the addition of CNTs [19, 20]. Several factors such as
53 surface conditions, epoxy types and CNT fractions, may have an impact on the lap shear
54 strength of CNT reinforced epoxy composites. Except those three influential factors, other
55 possible reasons for the inconsistency in previous studies may be accounted to the
56 geometry and material property differences of CNTs themselves.

57 The geometries of CNTs including diameter and length of the nanotubes. CNTs fall
58 into the category of nanomaterials because the diameter of the tubes is in nanometer scale,
59 but diameters also vary a lot from several nanometers to more than one hundred nanometers
60 [21]. Since the aspect ratio of CNTs is always extraordinary high, the length of CNTs is
61 typically far larger than the diameter. Due to different production methods, the length of
62 CNTs could be as short as micrometer level, or as long as centimeter level. The great
63 variances of CNTs' geometry in diameter and length inevitably result in extensive
64 differences in material properties and reinforcing efficiencies [7,22]. In the literature,
65 different researchers use CNTs with different geometries, very few researches involving
66 the effect of CNT geometries only focus on the thermal and electrical properties of CNT
67 reinforced epoxy composites [23,24]. To the best of the authors' knowledge, there is no

relevant research involving investigations on the influences of CNTs' geometries on mechanical properties, especially adhesion properties of CNT reinforced epoxy composites.

The dispersion characterizations of CNTs also play a key role to achieve good adhesion properties of CNT reinforced epoxy composites [25]. The high aspect ratio provides CNTs with remarkable mechanical properties, but also creates an enormous surface area of the tubes. The enormous surface area produces strong Van der Waals interactions which are responsible for the strong tendency of CNTs agglomeration [26]. The agglomerated CNTs have similar detrimental impact as defects and eventually reduce the adhesion properties of epoxy composites [27]. Therefore, a sufficient adhesion of CNT reinforced epoxy composites is directly related to the homogeneous dispersion of CNTs in the epoxy matrix [6, 28]. On the other hand, CNTs with different diameters and lengths have different aspect ratios, which naturally affect the dispersion characterizations of CNT reinforced epoxy composites [29]. The existing studies mostly report various approaches to improve the dispersion of CNTs with a certain geometry [30–32], there is a severe lack of relevant researches investigating dispersion characterizations of CNT reinforced epoxy composites with different CNT geometries.

In this paper, the effects of CNT geometries on the dispersion characterizations and adhesion properties of CNT reinforced epoxy composites were systematically investigated for the first time. CNTs with three different diameters, two different lengths, and three different weight fractions were compared regarding dispersion characterizations and adhesion properties, respectively. Specifically, particle size analysis was carried out to directly quantify the dispersion of CNTs. The adhesion properties of CNT reinforced epoxy composites including lap shear strength, fracture strain and toughness were examined by

single lap shear (SLS) tests. Transmission and scanning electron microscopy (TEM and SEM) were conducted on CNTs suspensions and fracture surfaces of CNT reinforced epoxy composites to reveal CNT distributions.

2. Experimental Investigations

2.1 Materials

Multi-walled CNTs with six different geometries including three different diameter ranges (10-12nm, 20-30nm, 50-100nm) and two different length ranges (normal-length range between 5 to 20μm, and short range between 0.5 to 2μm) were used in this study, labeled as N10, N20, N50, S10, S20, and S50. Table 1 shows the detailed geometries and other details of the six different types of CNTs according to the manufacturer's specification. All the CNTs were supplied by Skyspring Nanomaterials Inc (Houston, TX, USA) following the manufacturing method of Catalytic chemical vapor deposition. Pure acetone supplied by Sunnyside Corporation was used as solvent to disperse CNTs, since acetone is more volatile than ethanol or deionized water. Moreover, it is easier and faster to get rid of the acetone solution after mixing with epoxy resin. Standard all-purpose epoxy resin consisting of a bisphenol A based resin and a polyamide curing agent, was applied (supplied from East Coast Resin) as the composite matrix. The adherend material for making CNT reinforced epoxy adhesive joints was low carbon A36 steel supplied by Mid America Steel Inc.

Table 1 CNT geometries and other properties

Type	CNT Length (μm)	CNT Diameter (nm)	Specific surface area (m^2/g)	Purity (%)	Bulk density (g/cm^3)
N10	5-20 (Normal)	10-12	500	95	0.27
N20	5-20 (Normal)	20-30	110	95	0.28
N50	5-20 (Normal)	50-100	60	95	0.28
S10	0.5-2 (Short)	10-12	350	98	0.27

S20	0.5-2 (Short)	20-30	90	98	0.25
S50	0.5-2 (short)	50-100	70	98	0.18

2.2 Preparation of CNT suspensions

Although the most prevalent method of mixing CNTs is ultrasonic processing, it was found that the ultrasonic mixing may often induce the shortening of tube length and aspect ratio, which lead to differences in mechanical properties and other performances [33, 34]. Thus, in order to accurately investigate the effect of CNT geometries, ultrasonication was avoided during the mixing process. In this study, a new mixing protocol using a magnetic stirrer was developed to minimize alterations in CNT geometries and keep the CNTs intact. First of all, a conical flask filled with acetone was placed on the magnetic stirrer (supplied by Across International) and stirred by a magnetic rod at a speed of 1600 rpm, while CNTs with different geometries were gently added into the solvent. A commercially available surfactant called Sodium dodecylbenzene sulfonate (SDBS, obtained from Sigma-Aldrich Corp) with a constant weight fraction of 0.5% was also added into the solvent along with at least 2h mechanical stirring to make sure that CNTs were thoroughly dispersed. For each CNT geometry, suspensions with three different weight fractions (0.5%, 1%, and 2%) were examined to further investigate the effect of weight fractions on the dispersion characterizations of CNTs with different geometries.

2.3 Preparation of CNT reinforced epoxy composites

To prepare the CNT reinforced epoxy composites, the mechanical stirring CNT/acetone suspension was firstly mixed with the curing agent since the curing agent had less viscosity than the resin, followed by continually mechanical stirring on the stirrer for 2h to ensure a sufficient mixing between CNTs and curing agent. Then the whole mixture was placed in a vacuum at 80℃ for at least 4h to thoroughly remove the acetone. At last,

133 the CNT/curing agent mixture was mechanically mixed with the resin at a volume ratio of
134 1:1. The complete mixing protocols of CNT acetone suspensions and CNT reinforced
135 epoxy composites adopted in this study are illustrated in Fig. 1.

136 *2.4 Particle size analysis and SLS tests*

137 Particle size analysis is the most commonly used analytical testing method to directly
138 reveal the particle size distribution of CNTs in a wide range. In this study, the dispersion
139 characterizations of CNTs with different geometries were investigated by particle size
140 analysis using Particle Sizing Systems SPOS 780 as shown in Fig. 2(a).

141 In addition, SLS test specimens were designed and manufactured based on ASTM
142 D1002-10. The thickness of adherend sheets was enlarged to be 3.18mm to prevent
143 unexpected failure of the specimen resulted from early buckling of the sheets. Two
144 attachments were bonded at each end of the sheets to balance the misalignment. The
145 thickness of the epoxy composite layer between the two sheets was strictly controlled at
146 0.5 mm. SLS tests were carried out using the MTS Flex Test® SE loading frame under
147 monotonic tensile loading until shear failure occurred. The SLS test set-up is shown in Fig.
148 2(b), while the other specimen configurations, adherend pre-treatment methods, curing
149 conditions, as well as loading protocols were present in a previous study by the authors
150 [35]. For each testing condition, five identical specimens were manufactured and tested.
151 Table 2 demonstrates the experimental matrix to clearly present all the testing conditions
152 included in this study.

153 Table 2 Experimental matrix

Testing condition	CNT Length	CNT Diameter (nm)	CNT fraction (%)
N10-0.5	Normal	10-12	0.5
N10-1	Normal	10-12	1
N10-2	Normal	10-12	2

N20-0.5	Normal	20-30	0.5
N20-1	Normal	20-30	1
N20-2	Normal	20-30	2
N50-0.5	Normal	50-100	0.5
N50-1	Normal	50-100	1
N50-2	Normal	50-100	2
S10-0.5	Short	10-12	0.5
S10-1	Short	10-12	1
S10-2	Short	10-12	2
S20-0.5	Short	20-30	0.5
S20-1	Short	20-30	1
S20-2	Short	20-30	2
S50-0.5	Short	50-100	0.5
S50-1	Short	50-100	1
S50-2	Short	50-100	2

3. Results and discussions

3.1 Validation of CNT geometries with a new mixing protocol

Before discussing the dispersion characterizations of CNT reinforced epoxy composites with different CNT geometries, it is indispensable to find out if CNTs remained their initial geometries after the newly-developed mixing procedures, even though ultrasonication was not involved in the mixing protocol. Figs. 3(a ~ c) and Figs. 4(a, b) display TEM images of CNTs suspensions from different testing groups visualizing the diameters and lengths, respectively. As shown in Fig. 3, the typical diameters of CNTs from different testing groups (N10, N20, and N50) were around 10.3 nm, 25.0 nm, and 60.6 nm, respectively, which precisely matched the diameter range of the corresponding testing groups. Furthermore, as for the comparison of CNT lengths, it is clearly illustrated in Fig. 4 that CNTs from N20 group were generally much longer than CNTs from S20 group. Although it is quite difficult and time-consuming to accurately measure the length of all the individual CNTs, it is feasible to roughly estimate the average length of most CNTs in each figure by taking a few visible CNTs with most frequently lengths as

representatives. The estimated average length of CNTs in N20 and S20 group were around 10.4 μm and 1.4 μm, respectively, according to Fig.4. The average lengths of CNTs in those two testing groups were coincident with the corresponding original length range as well as the ratio between the two CNT geometries. Thus, both diameters and lengths of CNTs were not evidently affected by the mechanical stirring or the surfactant in the mixing protocol, indicating the validity of this new mixing protocol and experimental results in this study.

3.2 Dispersion characterizations

Figs. 5(a ~ c) illustrate the volume weighted particle size distributions of CNT suspensions of different CNT geometries with 0.5%, 1%, and 2% CNT fractions, respectively. The particle size corresponding to the peak in the distribution curve is called 'mode' describing the size with the highest frequency. As shown in Fig. 5, for CNT suspensions with all the testing conditions, two particle size distribution types were observed, namely unimodal distribution with only one mode and bimodal distributions with two modes [36]. For example, as shown in Fig 5(b), S10-1 (short CNTs with the diameter around 10 nm in 1% CNT fraction) showed a distribution type of unimodal since there was only one mode located at approximately 64 μm. While the distribution type of S20-1 (short CNTs with the diameter around 20 nm in 1% CNT fraction) belonged to bimodal distribution, with two modes occurring at around 12 μm and 33 μm, respectively. Table 3 summarizes the distribution types of all the testing conditions. In order to clearly and quantitatively demonstrate and compare the size distributions or dispersion with different CNT geometries and fractions, in Table 3, the statistical analysis of the particle distribution

191 in each testing condition was also presented, including the mode and geometric mean. The
192 geometric means were calculated using the equation below [33]:

$$D_{mean} = \sum_{i=1}^{n} (V_i \cdot D_i). \quad (1)$$

193 where, n is the number of particle size classes, V_i is the volume in percentage with class i,
194 and D_i is particle size of class i. It is generally believed that particle size distributions with
195 smaller mode sizes or smaller geometric means yield better dispersion. Because larger
196 particles confirm the existence of bigger CNT clusters as the result of non-uniform
197 dispersion.

198 Table 3 Particle size distribution and its statistical analysis

Testing condition	Distribution type	1st Mode (μm)	2nd Mode (μm)	Geometric mean (μm)
S10-0.5	Unimodal	37.93	/	31.29
S10-1	Unimodal	64.56	/	56.93
S10-2	Unimodal	101.43	/	87.78
S20-0.5	Bimodal	14.94	36.86	20.34
S20-1	Bimodal	13.32	48.23	28.46
S20-2	Bimodal	12.09	50.20	33.00
S50-0.5	Bimodal	12.65	41.81	20.26
S50-1	Bimodal	15.28	36.86	24.31
S50-2	Bimodal	11.09	42.05	29.95
N10-0.5	Bimodal	14.43	42.05	27.78
N10-1	Unimodal	66.82	/	52.06
N10-2	Unimodal	91.51	/	76.30
N20-0.5	Bimodal	11.81	38.15	14.10
N20-1	Bimodal	12.37	48.19	28.72
N20-2	Unimodal	50.78	/	38.36
N50-0.5	Unimodal	11.40	/	10.10
N50-1	Bimodal	13.09	47.96	20.67
N50-2	Bimodal	12.19	48.23	37.55

199 When comparing the particle size distributions of CNT suspensions with different
200 diameters, it is found that CNTs with larger diameters always had smaller mode sizes and
201 smaller geometric means, indicating the better dispersions of thicker CNTs, holding CNT
202 length and fraction the same. For instance, according to Fig. 5(a), N10-0.5, N20-0.5 shared

a same bimodal distribution. For N10-0.5, the volumes of 1st and 2nd mode were about less than 2% and 6%, respectively, implying that a larger proportion of CNTs had larger sizes. While for N20-0.5, the volumes of 1st and 2nd mode were about 5% and 3%, respectively. This volume change of the modes indicated that as the increase of CNT diameter, CNTs were more likely to exist in the form of smaller particles or clusters rather than larger ones. Moreover, from Table 3, the 1st and 2nd modes as well as the geometric mean of N20-0.5 were 11.81 μm, 38.15 μm, and 14.10 μm, which were all smaller than the corresponding values of N10-0.5 (14.43 μm, 42.05 μm, and 27.78 μm), respectively. For N50-0.5, when further enlarging the diameter of CNTs, the dispersion was continually improved. As shown in Fig. 5(a) and Table 3, the distribution type of N50-0.5 was converted into unimodal distribution with all the particles concentrating near the mode of 11.40 μm, and there was no larger particles or clusters to form the 2nd mode. It was evident that as the increase of CNT diameter, the particle size of CNTs in the suspension became smaller resulting in more uniform particle size distribution and dispersion. The same findings could also be drawn from CNTs with other lengths or fractions based on Fig. 5 and Table 3.

According to comparisons of particle size distributions between different lengths, the mode sizes and geometric means of CNTs with normal length were often smaller than short CNTs, holding the same CNT diameters and fractions. Take the comparisons between N20-1 and S20-1 as example as shown in Fig 5(b). Both of them had bimodal distributions, but the mode sizes and geometric mean of S10-2 were 13.32 μm, 48.23 μm, and 28.46 μm which were precisely close to those of N10-2 (12.37 μm, 48.19 μm, and 28.72 μm), respectively as shown in Table 3. Regarding most of the other testing conditions with the same CNT diameters and fractions, the distribution parameters of normal-length CNTs

were moderately smaller than short CNTs. On the contrary, there were also some cases that short CNTs had better particle size distribution than long CNTs, such as S0-2 and N20-2. In general, the differences of particle size distributions between normal-length and short CNTs were not significant enough to provide evident relationship between the dispersion states of CNTs with different lengths.

In addition to the effect of CNT geometries, the CNT fractions also had a considerable influence on the particle size distribution and dispersion of CNTs. By comparing CNTs with the same geometries but different percentages of additions, it was obvious that as the increase of CNT fractions, CNTs tended to have less uniform particle size distributions resulted from apparently larger distribution parameters. Because higher CNT fraction means more CNTs in a certain volume of solvent, leading to that CNTs are more likely to entangled together into larger CNT clusters.

The effects of CNT geometries and fractions on the dispersion characterizations could be verified by TEM images. Figs. 6(a ~ f) show the TEM images for the dispersion states of N10-2, N20-2, N50-2 (different diameters), S20-2 (different lengths), N20-0.5, and N20-1 (different fractions). According to Fig. 6(a) of N10-2, almost all the CNTs were entangled with each other into huge CNT clusters, and there were very few individual CNTs apart from those clusters. With the increase of CNT diameter as shown in Fig. 6(c) of N20-2, not only the size of cluster significantly reduced, but also many CNTs were separated from the medium-sized cluster, indicating a more uniform dispersion compared to N10-2. When further enlarging the CNT diameter to 50 nm as shown in Fig. 6(e) of N50-2, most of CNTs were relatively well dispersed with only two smaller clusters within the image area. Comparisons among CNTs with different diameters in the TEM images confirmed that

249 thicker CNTs were prone to have better dispersion characterizations than thinner CNTs.
250 With the same CNT additions, the reduction of CNT diameter increased the surface area
251 and aspect ratio of the tubes leading to stronger interaction among each CNT. Thus, CNTs
252 with small diameter are expected to aggregated tightly with each other yielding non-
253 uniform dispersion.

254 By comparing the TEM images of CNTs with different lengths as shown in Fig. 6(b)
255 and 6(e), N20-2 and S20-2 had similar dispersion characterizations with a CNT cluster
256 surrounded by many separate CNTs. However, the cluster size of N20-2 was fairly larger
257 than of S20-2 indicating the better dispersion of short CNTs, which was consistent with
258 the results from particle size analysis. The effect of CNT length on the dispersion was not
259 pronounced because the variation of length did not significantly change the surface area,
260 so that the attraction forces among each CNT nearly remained the same level. Therefore,
261 the dispersion characterizations of CNTs with different lengths were very similar.

262 Moreover, the comparisons of dispersion characterizations among CNTs with
263 different fractions were revealed by Figs. 6(b ~ d). It was evident that N20-0.5 and N20-1
264 were free of any clusters showing a more preferable dispersion than N20-2. Although there
265 was no noticeable difference between 0.5% and 1% CNT fractions, the dispersion
266 characterization of N20-0.5 seemed to be slightly better than that of N20-1. Since CNTs
267 with higher addition have higher possibility to interact or entangle with each other, it was
268 understood that higher CNT fractions normally exhibit non-uniform dispersion.

269 *3.3 Adhesion properties*

270 Adhesion properties are of top priority to the overall performance of epoxy
271 composites. It was initially believed that adhesion properties of CNT reinforced epoxy

composites with larger diameters should be better than that with smaller diameters, while CNT length may not have an obvious impact due to similar dispersion characterizations. Figs. 7(a ~ c) illustrate the average stress-strain curves of CNT reinforced epoxy composites among different CNT geometries with 0.5%, 1%, and 2% CNT fractions, respectively. The average stress-strain curve in each testing condition was mathematically fitted from the five curves measured from SLS tests. The fitting algorithm could be found in previous works by the authors [35, 37]. According to Fig. 7, all the curves shared a similar changing trend regardless of CNT geometries and fractions. As the increase of strain, the stress went up with a sharper slope at the beginning. After the strain reached at over 0.5, an inflection point was observed with the stress increasing remarkable slower and obviously dropping at the end. The shape of the stress-strain curves could be interpreted by pulling-out of the CNTs which is widely believed as one of the major reinforcing mechanisms of CNTs. At the beginning when the epoxy composites and CNTs were firmly bonded, they worked together as a strong integrity to bear the external loading. Owing to different moduli between epoxy and CNTs, when the strain increased to the ultimate shear strain of epoxy, the epoxy matrix was fractured and deactivated, which reduced the overall shear modulus. Although a part of CNTs started to be pulled-out from the surrounding epoxy matrix, the rest part kept well bonded and continually worked to bear the loading. As the pulling-out part extended, the remaining CNTs were not able to bear the loading, catastrophic fracture occurred and CNT reinforced epoxy composites failed [19, 38].

The lap shear strength was identified as the highest stress in the stress-strain curves. Figs. 8(a ~ c) show the lap shear strengths of CNT reinforced epoxy composites among different geometries with 0.5%, 1%, and 2% CNT fractions, respectively. As shown in Fig.

8(a), the lap shear strength of N20-0.5 (normal length, 20 nm diameter and 0.5% CNT fraction) was 28.30 MPa which was slightly higher than that of N10-0.5. After further increasing the diameter to 50 nm, the lap shear strength reached 29.90 MPa with about 8% increase compared to N10-0.5. For CNT reinforced epoxy composites with the other lengths and fractions, similar increasing trends were observed. The most noteworthy improvement was obtained by N50-1, with increase of around 22% compared to N10-1. It was known that the dispersion characterization of CNTs had a decisive effect on the lap shear strength and adhesion properties of CNT reinforced epoxy composites, and CNTs with larger diameters normally have better dispersion characterizations [25]. Therefore, it was validified that the epoxy composites reinforced by thicker CNTs tend to have higher lap shear strength due to the more uniform dispersion.

As for the influence of CNT length on the lap shear strength of CNT reinforced epoxy composites, it was obvious in Fig. 8 that with the same CNT diameters and fractions, the lap shear strengths of epoxy composites reinforced by normal-length CNTs were much higher than those reinforced by short CNTs. Especially, the lap strength of N10-0.5 was almost twice as much as that of S10-0.5. Furthermore, it was noted that the lap shear strength of N10-0.5 was even a little higher than that of S50-0.5, and this trend was valid for the other CNT fractions of 1% and 2%. Given that the dispersion characterizations of S50-0.5, S50-1, and S50-2 were much better than those of N10-0.5, N10-1, and N10-2 respectively as shown in Fig. 5 and Table 3, the initial hypothesis of the insignificant effect of CNT length was not applicable with regard to adhesion properties. Epoxy composites reinforced by longer CNTs yielding stronger lap shear strengths cannot be simply explained by the effect of dispersion characterization. It was reported in the literature [39,

40] that CNTs with very small lengths were difficult to accomplish a sufficient stress transfer between them and the surrounding epoxy matrix. When lacking interfacial bonding and anchoring on the CNT-epoxy interface, short CNTs were expected to have the similar detrimental effect as imperfections which reduced the stiffness and continuity of the epoxy matrix [41]. On the other hand, by comparing the lap shear strength of CNT reinforced epoxy composites with different CNT fractions, as the increase of CNT addition, the lap shear strength kept dropping due to more non-uniform CNT dispersion.

In addition to lap shear strength, the area under the stress-strain curve could be integrated as toughness which is another important adhesion parameter describing the ability of energy absorption and plastic deformation. Based on Fig. 7, Figs. 9(a ~ c) show the comparisons of toughness among CNT reinforced epoxy composites with different geometries and fractions. Similar as the changing trend of lap shear strength, as the increase of CNT diameter, the toughness of CNT reinforced epoxy composites also improved. As shown in Fig. 9(a), the toughness of N50-0.5 was 36% and 22% higher than those of N50-0.5 and N50-1, respectively. The most tremendous enhancement was also achieved by N50-1, with the increments reaching 54% compared to N10-1. It was worth noting that nearly all the increments in toughness with the same testing conditions were more significant than those in lap shear strength. Considering toughness is determined by both strength and ductility, the increase of CNT diameter not only improved the lap shear strength, but also enhanced the deformability and ductility of CNT reinforced epoxy composites.

When comparing CNT reinforced epoxy composites with the same CNT diameter and fractions but different lengths, Fig. 9 demonstrates that the toughness of epoxy composites

reinforced by normal-length CNTs was always markedly better than those by short CNTs. The improvement in toughness of N50-1 was as much as 52% higher compared to S50-1 in particular. The variation in toughness between epoxy composites reinforced by normal-length and short CNTs might be attributed to the same mechanism in lap shear strength as discussed above. Since insufficient stress transfer between short CNTs and epoxy leading to discontinuity and imperfections of the matrix as a whole, undoubtedly the toughness of short CNT reinforced epoxy composites was rather limited. Moreover, the changing trend of CNT fractions in lap shear strength was still valid in toughness. As the increase of CNT fraction, the toughness of CNT reinforced epoxy composites decreased as a results of non-uniform CNT dispersion.

3.4 SEM analysis on fracture surfaces

To further investigate the dispersion state of CNTs into the epoxy matrix as well as understanding the mechanisms of CNT geometries behind the experimental data, SEM images were also taken on the fracture surfaces of epoxy composites as illustrated in Figs. 10(a ~ f) including N10-0.5, N20-0.5, N50-0.5 (different diameters), S50-0.5 (different length), N50-1 and N50-2 (different fractions). It was found in Fig. 10(a) for N10-0.5 that there was a huge CNT clusters with the estimated diameter of 28.0 μm, along with several small clusters. With the increase of CNT diameter for N20-0.5 as shown in Fig. 10(c), the size of the biggest CNT cluster reduced significantly to around 14 μm, and further reduced to around 10.0 μm for N50-0.5 as shown in Fig. 10(e). It was confirmed that epoxy composites reinforced by thicker CNTs had better dispersion which contributed to better lap shear strength and toughness.

Fig. 10(e) and 10(f) compare the typical SEM images of CNT reinforced epoxy composites with different lengths. The sizes of CNT clusters of N50-0.5 were visibly smaller than those of S50-0.5 indicating the better dispersion characterizations and adhesion properties of epoxy composites reinforced by normal-length CNTs. By comparing N50-0.5, N50-1, and N50-2 as shown in Fig. 10(b), 10(d), and 10(e), CNT reinforced epoxy composites with lower CNT fraction had smaller clusters leading to more uniform CNT dispersion and stronger adhesion. In general, the sizes of CNT clusters demonstrated in each SEM image were consistent with the measurements in particle size analysis, which proved the validation and accuracy of the experimental results. Except those CNT clusters, there was also a great deal of individual CNTs as demonstrated in Fig. 10(b) as well as other figures. Although those thoroughly and homogeneously dispersed CNTs overnumbered CNT clusters a lot, the global dispersion characterization was still dominated by CNT clusters.

The SEM images of N10-0.5 and N50-0.5 as shown in Fig. 10(a) and 10(c) were further scanned at high magnification as shown in Figs. 11(a, b). It was observed in Fig. 11(a) that the phenomenon of CNT pulling-out was not significant. For most visible CNTs, the main part of the length was still buried into the epoxy with only a tip exposed above the matrix surface. However, as shown in Fig. 11(b), a large part of CNTs had been considerably pulled out from the epoxy matrix, although the pulled-out length varied with each individual CNT. The process of CNT pulling-out was discussed in the last section. Since a lot of energy was consumed by the pulled-out CNTs, this comparison verified that the toughness of CNT reinforced epoxy composites with larger CNT diameters was higher than that with thinner ones, and similar phenomena could also be found between CNT

reinforced epoxy composites with different CNT lengths and fractions. It was noted that more CNT pulling-outs prompted the energy consumption, improved the toughness and eventually resulted in better adhesion properties.

4. Conclusions

The main objective of this study was to investigate the effects of CNT geometries on the dispersion characterizations and adhesion properties of CNT reinforced epoxy composites. CNTs with different geometries were dispersed into pure acetone solution by a new mixing protocol, and dispersion characterizations of the CNT suspensions were studied by particle size analysis and TEM. The adhesion properties of CNT reinforced epoxy composites were exanimated by single lap shear (SLS) tests and SEM. Based on the findings, following conclusions can be drawn:

(1) The TEM analysis confirmed that the diameter and length of CNTs were not evidently affected by newly-developed mixing protocol. After the mixing process, CNTs were able to keep their original diameters and lengths.

(2) CNT suspensions with larger CNT diameters were more likely to have smaller particle size as a result of better dispersion characterizations. This was because smaller CNTs exhibited larger surface area and aspect ratio which normally resulted in stronger interaction to entangle CNTs together as CNT clusters.

(3) Due to the more uniform dispersion of CNTs, epoxy composites reinforced by thicker CNTs had better adhesion properties not only in the higher lap shear strength but also higher toughness implying better ductility and deformability.

(4) For the effect of CNT length, according to both particle size and TEM analysis, there was no evident difference between the dispersion characterizations of CNT

suspensions with normal-length and short CNTs. Since the variance of CNT length did not significantly change the surface area of CNTs, so that the attraction forces among each CNT nearly remained the same level. However, the adhesion properties of CNT reinforced epoxy composites with normal-length CNTs were much better than those with short CNTs, with the increments could reach as much as 100% in lap shear strength and 52% in toughness. In addition, as the increase of CNT fractions, both dispersion characterizations and adhesion properties deteriorated owing to severe CNT agglomeration.

As the findings from this paper indicated that the geometries of CNTs indeed influence quite significantly on the dispersion and properties CNT reinforced epoxy composites, for these composites, investigations related to property improvements are recommended to provide details on the used CNTs for better understandings on the effects for future related studies.

CRediT authorship contribution statement

Dawei Zhang: Data curation, Methodology, Formal analysis, Investigation, Writing - original draft, Writing - review & editing. **Ying Huang**: Project administration, Funding acquisition, Supervision, Writing - review & editing. **Leonard Chia**: Methodology, Investigation.

Declaration of interest

The authors declare that they have no known competing financial interests or personal relationships that could have appeared to influence the work reported in this paper.

Acknowledgements

This work was supported the National Science Foundation under Grant No. CMMI-1750316. The findings and opinions expressed in this article are those of the authors only and do not necessarily reflect the views of the sponsors.

Reference

[1] S. Iijima, Helical Microtubules of Graphitic Carbon, Nature 354 (1991) 56-58. https://doi.org/10.1038/354056a0

[2] A. Kausar, I. Rafique, B. Muhammad, Review of Applications of Polymer/Carbon Nanotubes and Epoxy/CNT Composites, Polym. - Plast. Technol. Eng. 55 (2016) 1167–1191. https://doi.org/10.1080/03602559.2016.1163588.

[3] J.N. Coleman, U. Khan, W.J. Blau, Y.K. Gun'ko, Small but strong: A review of the mechanical properties of carbon nanotube-polymer composites, Carbon N. Y. 44 (2006) 1624–1652. https://doi.org/10.1016/j.carbon.2006.02.038.

[4] Y. Liu, S. Kumar, Polymer/carbon nanotube nano composite fibers-A review, in: ACS Appl. Mater. Interfaces. 6 (2014) 6069-6087. https://doi.org/10.1021/am405136s.

[5] Q. Zhao, X. Gan, K. Zhou, Enhanced properties of carbon nanotube-graphite hybrid-reinforced Cu matrix composites via optimization of the preparation technology and interface structure, Powder Technol. 355 (2019) 408–416. https://doi.org/10.1016/j.powtec.2019.07.055.

[6] G. Pandey, E.T. Thostenson, Carbon nanotube-based multifunctional polymer nanocomposites, Polym. Rev. 52 (2012) 355–416. https://doi.org/10.1080/15583724.2012.703747.

[7] M.R. Zakaria, M.H. Abdul Kudus, H.Md. Akil, M.Z.Mohd Thirmizir. Comparative study of graphene nanoparticle and multiwall carbon nanotube filled epoxy nanocomposites based on mechanical, thermal and dielectric properties. Compos. Part B Eng. 119 (2017) 57–66. https://doi.org/10.1016/j.compositesb.2017.03.023.

[8] M.R. Zakaria, M.H. Abdul Kudus, H.Md. Akil, M.Z.Mohd Thirmizir, M.F.I. Abdul Malik, M.B. Hafi Othman, F. Ullah, F. Javed. Comparative study of single-layer graphene and single-walled carbon nanotube-filled epoxy nanocomposites based on mechanical and thermal properties. Polym. Compos. 40 (2018) E1840-1849. https://doi.org/10.1002/pc.25173.

[9] A. Anvari, The Influence of CNT Structural Parameters on the Properties of CNT and CNT-Reinforced Epoxy, Int. J. Aerosp. Eng. 2020 (2020). https://doi.org/10.1155/2020/4873426.

[10] D. Zhang, Y. Huang, Y. Wang, Bonding performances of epoxy coatings reinforced by carbon nanotubes (CNTs) on mild steel substrate with different surface roughness, Compos. Part A Appl. Sci. Manuf. 147 (2021) 106479. https://doi.org/10.1016/j.compositesa.2021.106479.

[11] S.R. Nayak, K.N.S. Mohana, M.B. Hegde, K. Rajitha, A.M. Madhusudhana, S.R. Naik, Functionalized multi-walled carbon nanotube/polyindole incorporated epoxy: An effective anti-corrosion coating material for mild steel, J. Alloys Compd. 856 (2021) 158057. https://doi.org/10.1016/j.jallcom.2020.158057.

[12] H. Hu, Y. He, Z. Long, Y. Zhan, Synergistic effect of functional carbon nanotubes and graphene oxide on the anti-corrosion performance of epoxy coating, Polym.

Adv. Technol. 28 (2017) 754–762. https://doi.org/10.1002/pat.3977.

[13] M. Konstantakopoulou, G. Kotsikos, Effect of MWCNT filled epoxy adhesives on the quality of adhesively bonded joints, Plast. Rubber Compos. 45 (2016) 166–172. https://doi.org/10.1080/14658011.2016.1165788.

[14] X. Wu, K. He, Z. Gong, Z. Liu, J. Jiang, The shear strength of composite secondary bonded single-lap joints with different fabrication methods, J. Adhes. Sci. Technol. 34 (2020) 936–948. https://doi.org/10.1080/01694243.2019.1690775.

[15] A.M. Pereira, J.M. Ferreira, F. V. Antunes, P.J. Bártolo, Analysis of manufacturing parameters on the shear strength of aluminium adhesive single-lap joints, J. Mater. Process. Technol. 210 (2010) 610–617. https://doi.org/10.1016/j.jmatprotec.2009.11.006.

[16] L.D.R. Grant, R.D. Adams, L.F.M. da Silva, Experimental and numerical analysis of single-lap joints for the automotive industry, Int. J. Adhes. Adhes. 29 (2009) 405–413. https://doi.org/10.1016/j.ijadhadh.2008.09.001.

[17] A. Kumar, K. Kumar, P.K. Ghosh, A. Rathi, K.L. Yadav, Raman, MWCNTs toward superior strength of epoxy adhesive joint on mild steel adherent, Compos. Part B Eng. 143 (2018) 207–216. https://doi.org/10.1016/j.compositesb.2018.01.016.

[18] P. Jojibabu, M. Jagannatham, P. Haridoss, G.D. Janaki Ram, A.P. Deshpande, S.R. Bakshi, Effect of different carbon nano-fillers on rheological properties and lap shear strength of epoxy adhesive joints, Compos. Part A Appl. Sci. Manuf. 82 (2016) 53–64. https://doi.org/10.1016/j.compositesa.2015.12.003.

[19] M.R. Ayatollahi, A. Nemati Giv, S.M.J. Razavi, H. Khoramishad, Mechanical properties of adhesively single lap-bonded joints reinforced with multi-walled carbon nanotubes and silica nanoparticles, J. Adhes. 93 (2017) 896–913. https://doi.org/10.1080/00218464.2016.1187069.

[20] S.M.J. Razavi, M.R. Ayatollahi, A. Nemati Giv, H. Khoramishad, Single lap joints bonded with structural adhesives reinforced with a mixture of silica nanoparticles and multi walled carbon nanotubes, Int. J. Adhes. Adhes. 80 (2018) 76–86. https://doi.org/10.1016/j.ijadhadh.2017.10.007.

[21] J.-P. Salvetat, J.-M. Bonard, N.H. Thomson, A.J. Kulik, L. Forró, W. Benoit, L. Zuppiroli, Mechanical properties of carbon nanotubes, Appl. Phys. A. 69 (1999) 255–260. https://doi.org/10.1007/s003399900114.

[22] E. Mainini, H. Murakawa, P. Piovano, U. Stefanelli, Carbon-nanotube geometries as optimal configurations, Multiscale Model. Simul. 15 (2017) 1448–1471. https://doi.org/10.1137/16M1087862.

[23] W.S. Bao, S.A. Meguid, Z.H. Zhu, Y. Pan, G.J. Weng, Effect of carbon nanotube geometry upon tunneling assisted electrical network in nanocomposites, J. Appl. Phys. 113 (2013) 234313. https://doi.org/10.1063/1.4809767.

[24] R.J. Warzoha, A.S. Fleischer, Effect of carbon nanotube interfacial geometry on thermal transport in solid-liquid phase change materials, Appl. Energy. 154 (2015) 271–276. https://doi.org/10.1016/j.apenergy.2015.04.121.

[25] S.A. Sydlik, J.H. Lee, J.J. Walish, E.L. Thomas, T.M. Swager, Epoxy functionalized multi-walled carbon nanotubes for improved adhesives, Carbon N. Y. 59 (2013) 109–120. https://doi.org/10.1016/j.carbon.2013.02.061.

[26] A. Thess, R. Lee, P. Nikolaev, H. Dai, P. Petit, J. Robert, Crystalline ropes of metallic carbon nanotubes, Science. 273 (1996) 483-487. https://doi.org/10.1126/science.273.5274.483

[27] E. Gao, W. Lu, Z. Xu, Strength loss of carbon nanotube fibers explained in a three-level hierarchical model, Carbon N. Y. 138 (2018) 134–142. https://doi.org/10.1016/j.carbon.2018.05.052.

[28] J.N. Coleman, U. Khan, Y.K. Gun'ko, Mechanical reinforcement of polymers using carbon nanotubes, Adv. Mater. 18 (2006) 689–706. https://doi.org/10.1002/adma.200501851.

[29] A.H. Korayem, M.R. Barati, S.J. Chen, G.P. Simon, X.L. Zhao, W.H. Duan, Optimizing the degree of carbon nanotube dispersion in a solvent for producing reinforced epoxy matrices, Powder Technol. 284 (2015) 541–550. https://doi.org/10.1016/j.powtec.2015.07.023.

[30] H. Yang, Y. Yang, Y. Liu, D. He, J. Bai, Multi-scale study of CNT and CNT-COOH reinforced epoxy composites: dispersion state, interfacial interaction vs mechanical properties, Compos. Interfaces. 28 (2021) 381–393. https://doi.org/10.1080/09276440.2020.1780556.

[31] M.D. Shokrian, K. Shelesh-Nezhad, R. Najjar, Effect of CNT dispersion methods on the strength and fracture mechanism of interface in epoxy adhesive/Al joints, J. Adhes. Sci. Technol. 33 (2019) 1394–1409. https://doi.org/10.1080/01694243.2019.1595304.

[32] P.C. Ma, S.Y. Mo, B.Z. Tang, J.K. Kim, Dispersion, interfacial interaction and re-agglomeration of functionalized carbon nanotubes in epoxy composites, Carbon N.

Y. 48 (2010) 1824–1834. https://doi.org/10.1016/j.carbon.2010.01.028.

[33] K.G. Dassios, P. Alafogianni, S.K. Antiohos, C. Leptokaridis, N.M. Barkoula, T.E. Matikas, Optimization of sonication parameters for homogeneous surfactant assisted dispersion of multiwalled carbon nanotubes in aqueous solutions, J. Phys. Chem. C. 119 (2015) 7506–7516. https://doi.org/10.1021/acs.jpcc.5b01349.

[34] G. Gkikas, N.M. Barkoula, A.S. Paipetis, Effect of dispersion conditions on the thermo-mechanical and toughness properties of multi walled carbon nanotubes-reinforced epoxy, in: Compos. Part B Eng., 2012: pp. 2697–2705. https://doi.org/10.1016/j.compositesb.2012.01.070.

[35] D. Zhang, Y. Huang, The bonding performances of carbon nanotube (CNT)-reinforced epoxy adhesively bonded joints on steel substrates, Prog. Org. Coatings. 159 (2021) 106407. https://doi.org/10.1016/j.porgcoat.2021.106407.

[36] S. Parveen, S. Rana, R. Fangueiro, M.C. Paiva, Characterizing dispersion and long term stability of concentrated carbon nanotube aqueous suspensions for fabricating ductile cementitious composites, Powder Technol. 307 (2017) 1–9. https://doi.org/10.1016/j.powtec.2016.11.010.

[37] D. Zhang, Y. Huang, Influence of surface roughness and bondline thickness on the bonding performance of epoxy adhesive joints on mild steel substrates, Prog. Org. Coatings. 153 (2021) 106135. https://doi.org/10.1016/j.porgcoat.2021.106135.

[38] X. Chen, I.J. Beyerlein, L.C. Brinson, Curved-fiber pull-out model for nanocomposites. Part 1: Bonded stage formulation, Mech. Mater. 41 (2009) 279–292. https://doi.org/10.1016/j.mechmat.2008.12.004.

[39] A. Haque, A. Ramasetty, Theoretical study of stress transfer in carbon nanotube

reinforced polymer matrix composites, Compos. Struct. 71 (2005) 68–77. https://doi.org/10.1016/j.compstruct.2004.09.029.

[40] M.M. Shokrieh, R. Rafiee, Investigation of nanotube length effect on the reinforcement efficiency in carbon nanotube based composites, Compos. Struct. 92 (2010) 2415–2420. https://doi.org/10.1016/j.compstruct.2010.02.018.

[41] V. V. Mokashi, D. Qian, Y. Liu, A study on the tensile response and fracture in carbon nanotube-based composites using molecular mechanics, Compos. Sci. Technol. 67 (2007) 530–540. https://doi.org/10.1016/j.compscitech.2006.08.014.

Figure captions

Fig. 1 The complete mixing procedures: (a) CNT suspensions; (b) CNT reinforced epoxy composites.

Fig. 2 Test set-up: (a) Particle size analysis; (b) SLS test.

Fig. 3 TEM images showing the diamters of CNTs: (a) N10; (b) N20; (c) N50

Fig. 4 TEM images showing the lengths CNTs: (a) N20; (b) S20

Fig. 5 Volume weighted particle size distributions of CNT suspensions of different CNT geometries: (a) 0.5%; (b) 1%; (c) 2% CNT fractions

Fig. 6 TEM images showing the real dispersion states of CNTs with different geometries and fractions: (a): N10-2; (b) N20-0.5; (c) N20-2; (d) N20-1; (e) N50-2; (f) S20-2

Fig. 7 Average stress-strain curves of CNT reinforced epoxy composites with different CNT geometries: (a) 0.5%; (b) 1%; (c) 2% CNT fractions

Fig. 8 Lap shear strenths of CNT reinforced epoxy composites with different CNT geometries: (a) 0.5%; (b) 1%; (c) 2% CNT fractions

Fig. 9 Toughness of CNT reinforced epoxy composites with different CNT geometries: (a) 0.5%; (b) 1%; (c) 2% CNT fractions

Fig. 10 SEM images on the fracutre surfaces of CNT reinforced epoxy composites: (a) N10-0.5; (b) N20-1; (c) N20-0.5; (d) N20-2; (e) N50-0.5; (f) S50-0.5.

Fig. 11 SEM images at high magnification: (a) N10-0.5; (b) N50-0.5

596

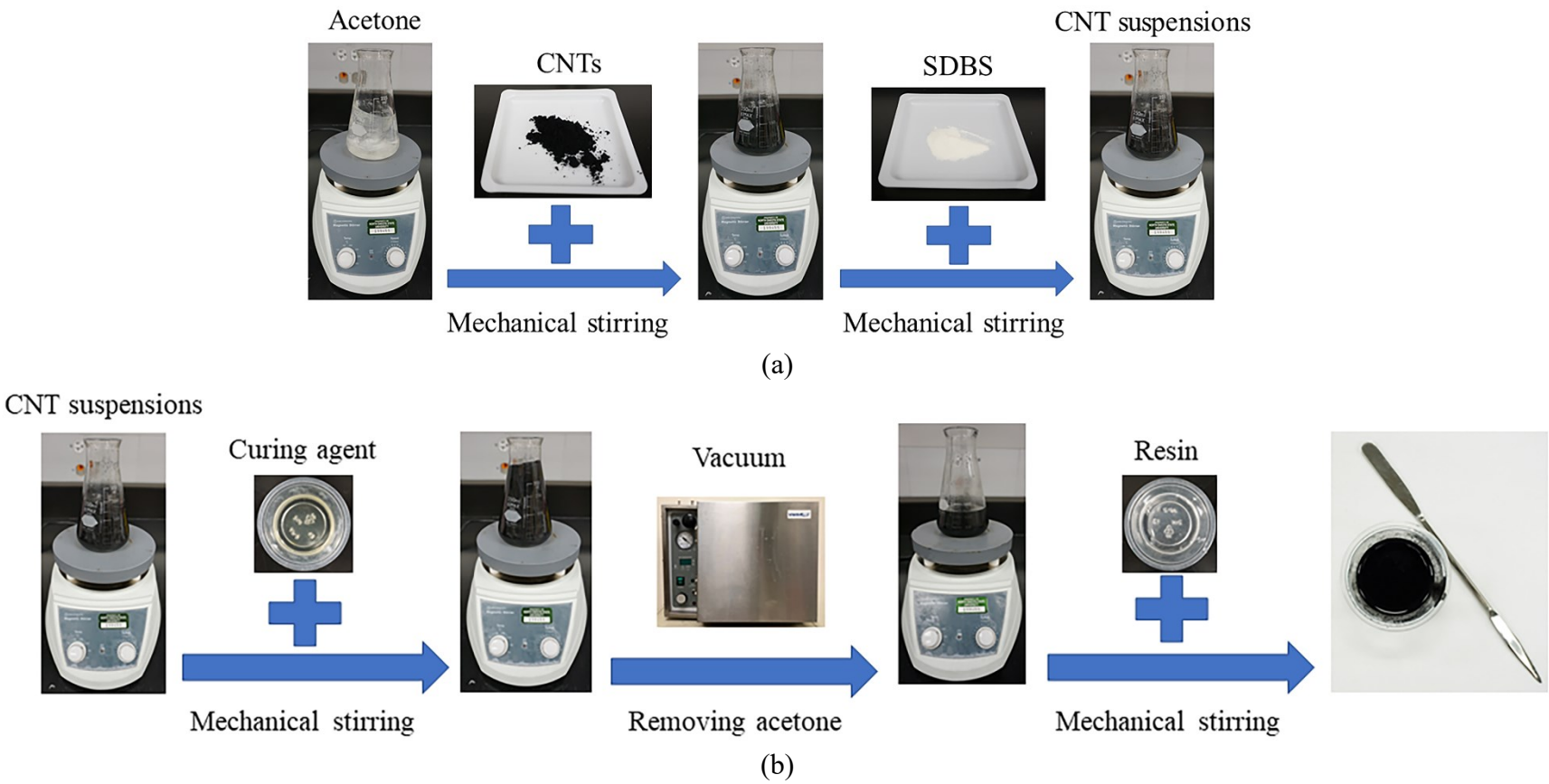

597 Fig.1 The complete mixing procedures: (a) CNT suspensions; (b) CNT reinforced epoxy composites

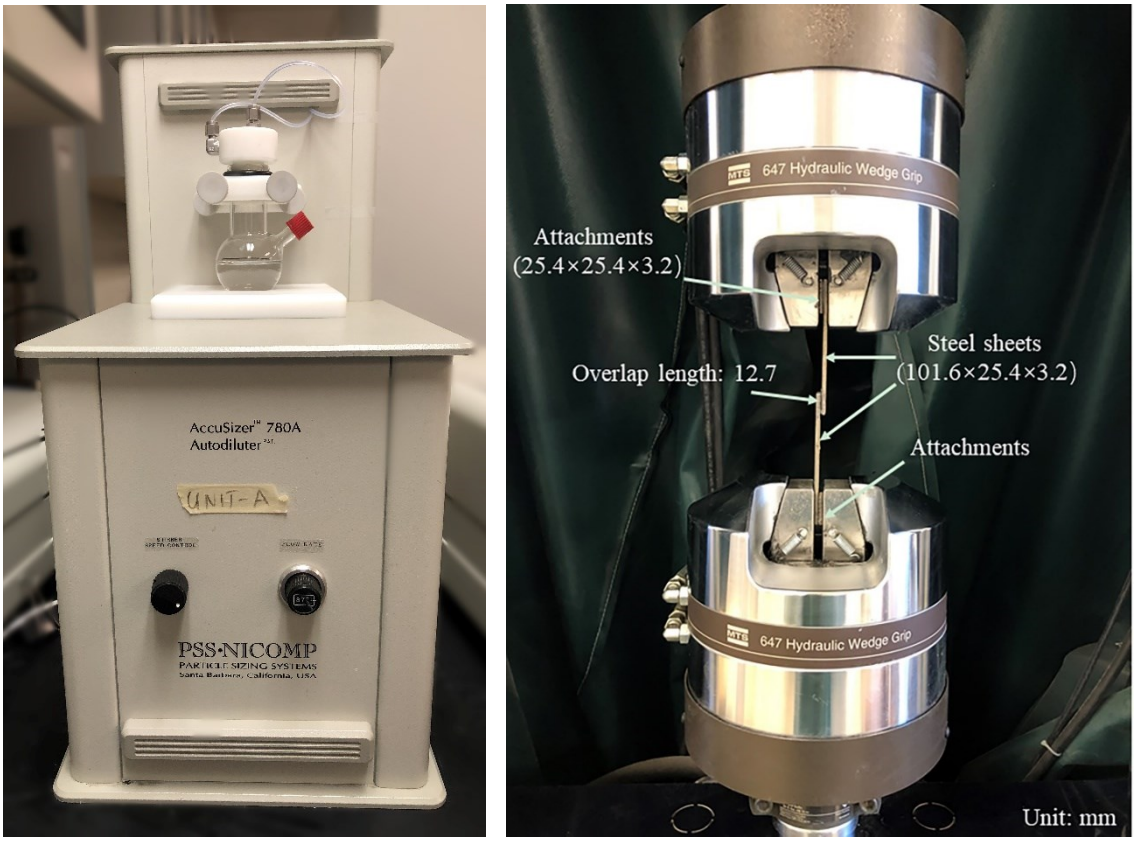

(a) (b)

598 Fig.2 Test set-up: (a) Particle size analysis; (b) SLS test

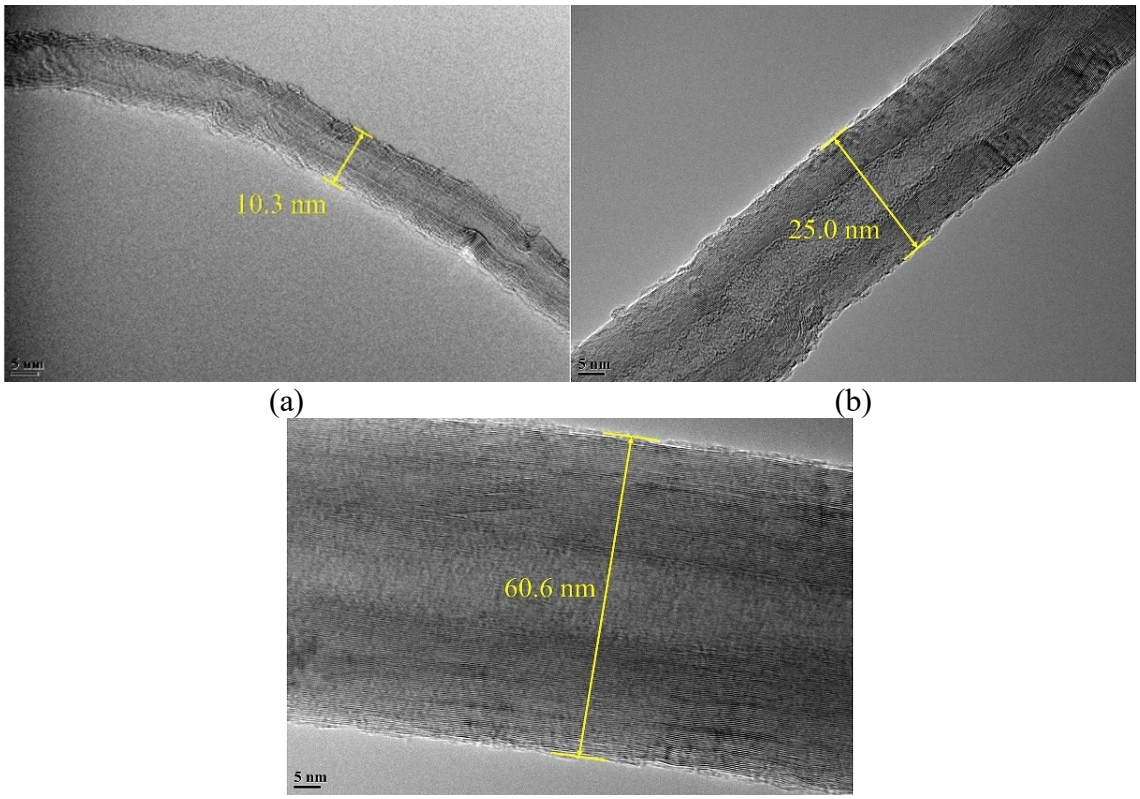

(a) (b)

(c)

599 Fig. 3 TEM images showing the diamters of CNTs: (a) N10; (b) N20; (c) N50.

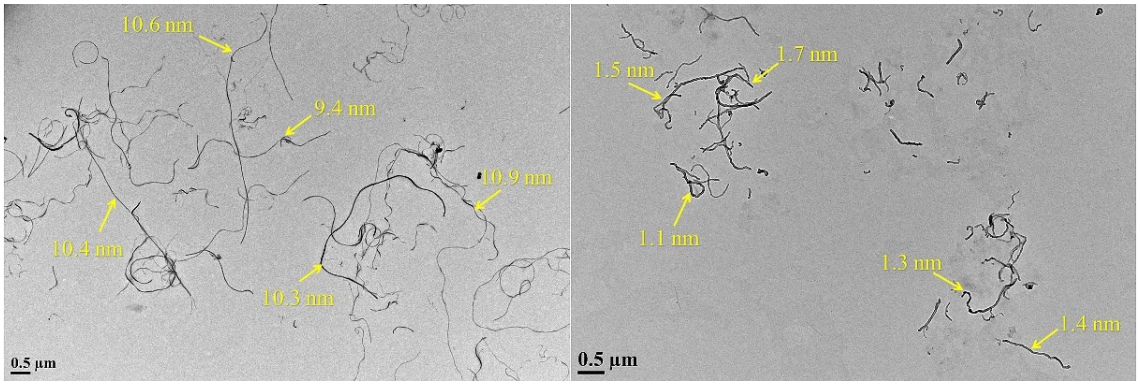

(a) (b)

600 Fig. 4 TEM images showing the lengths CNTs: (a) N20; (b) S20.

601

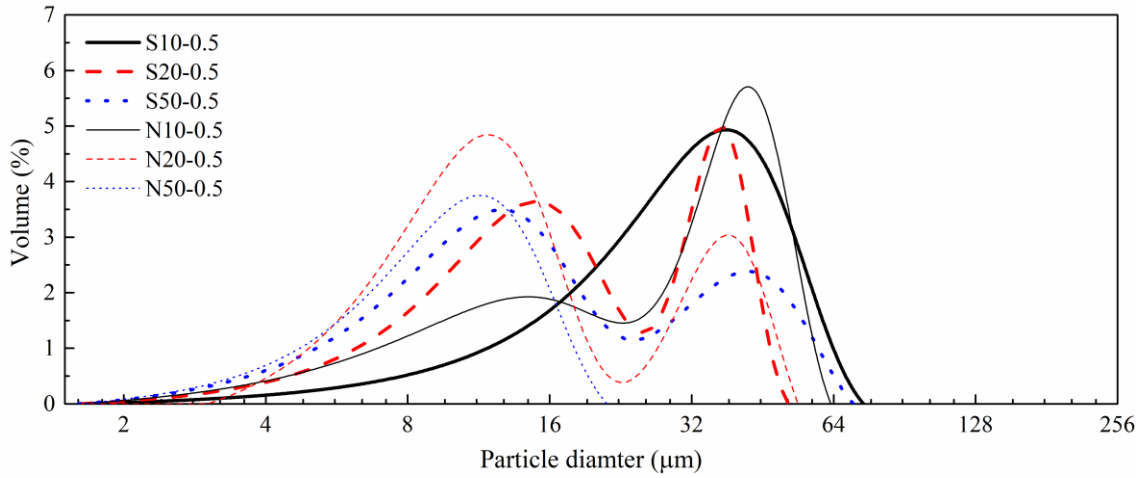

(a)

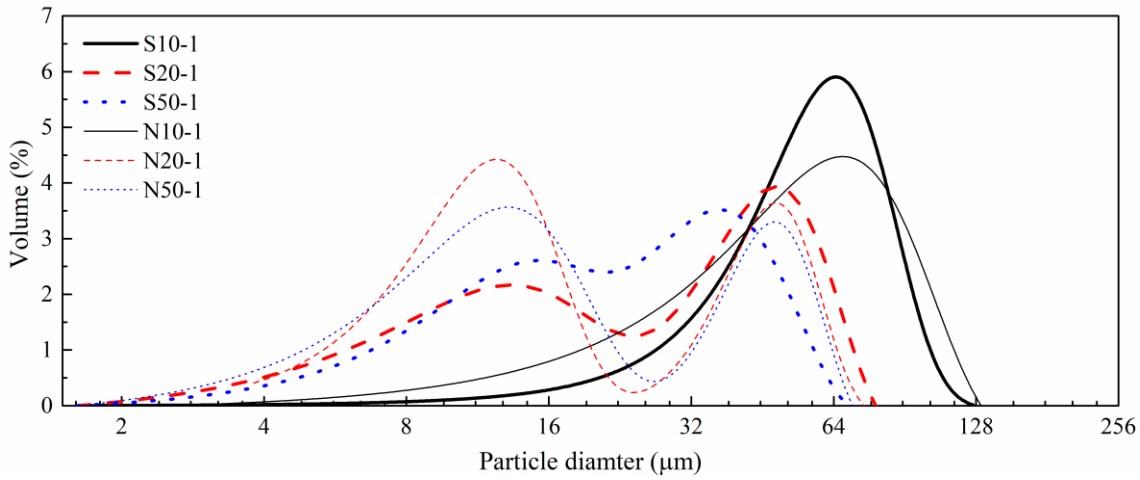

(b)

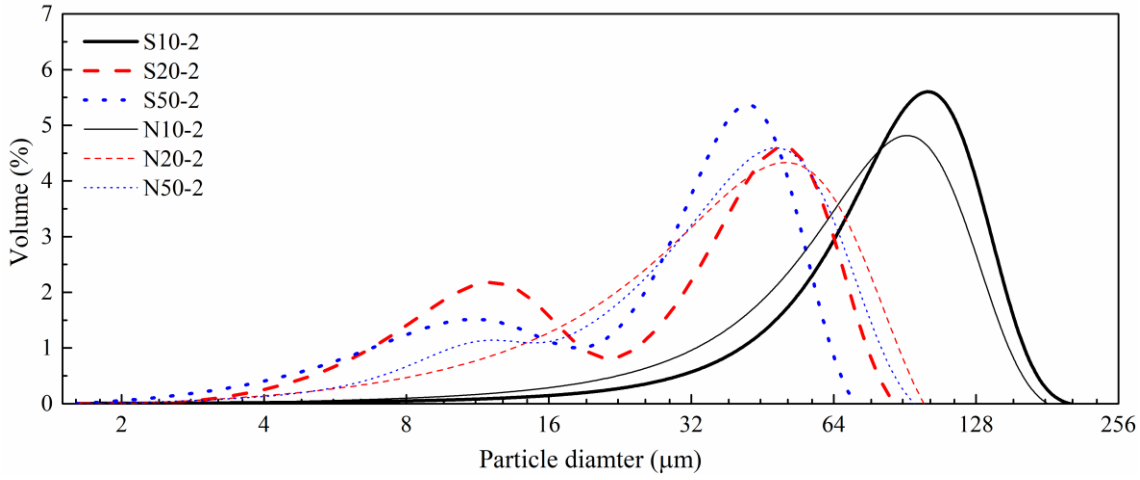

(c)

602 Fig. 5 Volume weighted particle size distributions of CNT suspensions of different CNT
603 geometries: (a) 0.5%; (b) 1%; (c) 2% CNT fractions.

604

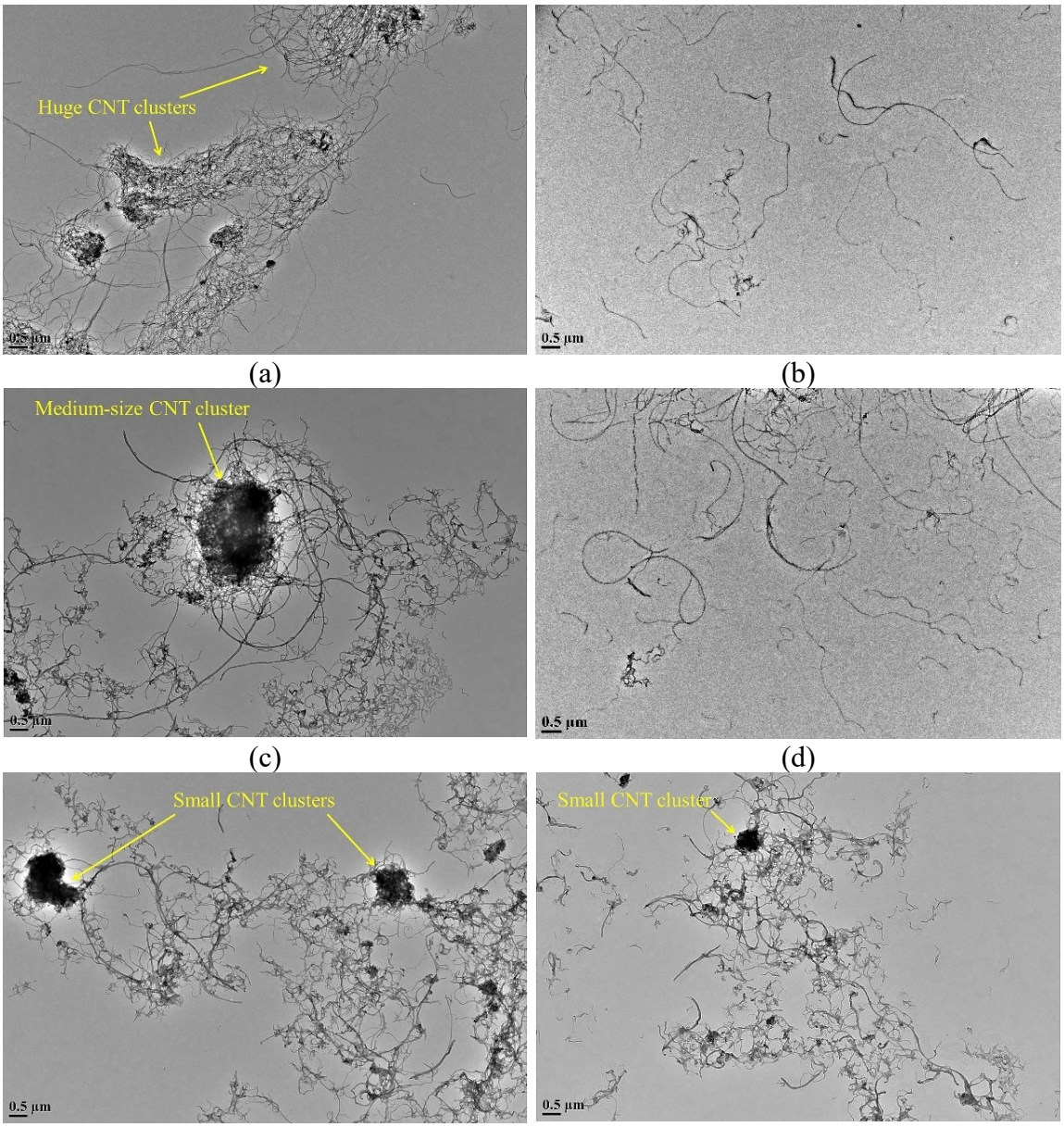

Fig. 6 TEM images showing the real dispersion states of CNTs with different geometries and fractions: (a) N10-2; (b) N20-0.5; (c) N20-2; (d) N20-1; (e) N50-2; (f) S20-2.

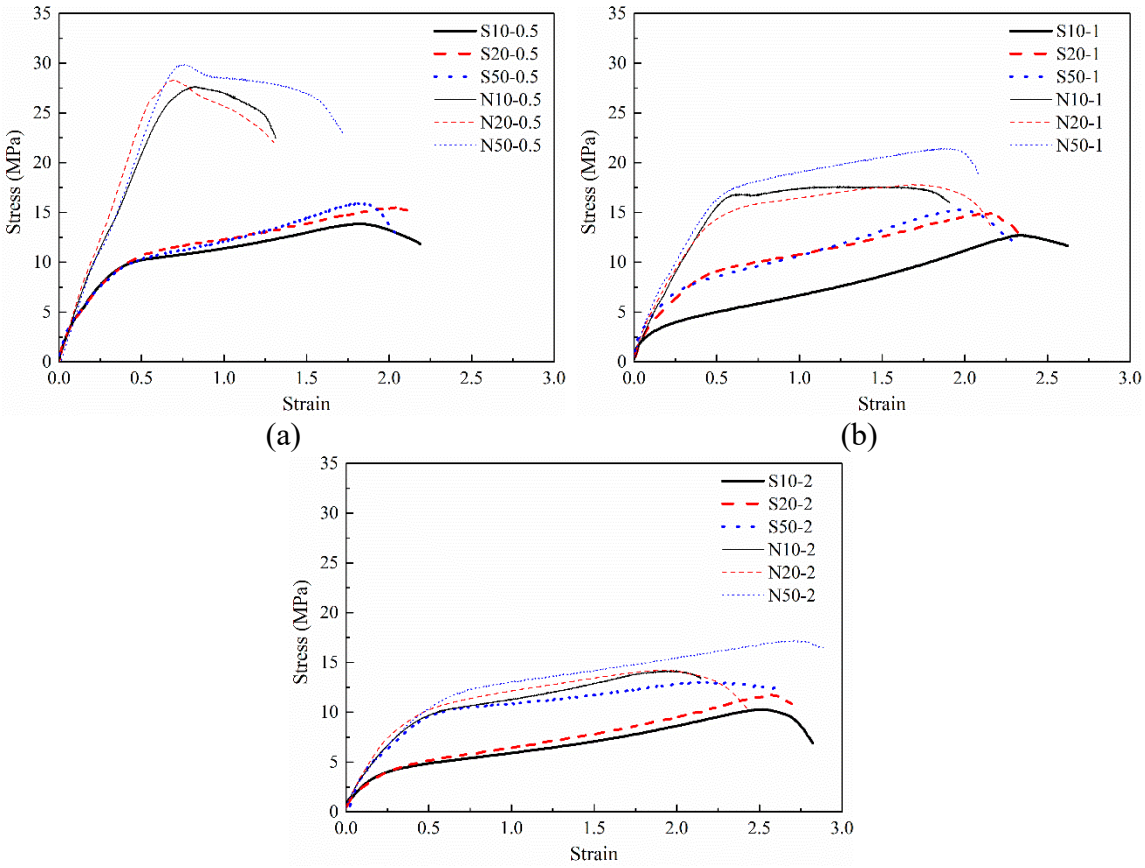

608 Fig. 7 Average stress-strain curves of CNT reinforced epoxy composites with different
609 CNT geometries: (a) 0.5%; (b) 1%; (c) 2% CNT fractions.

610

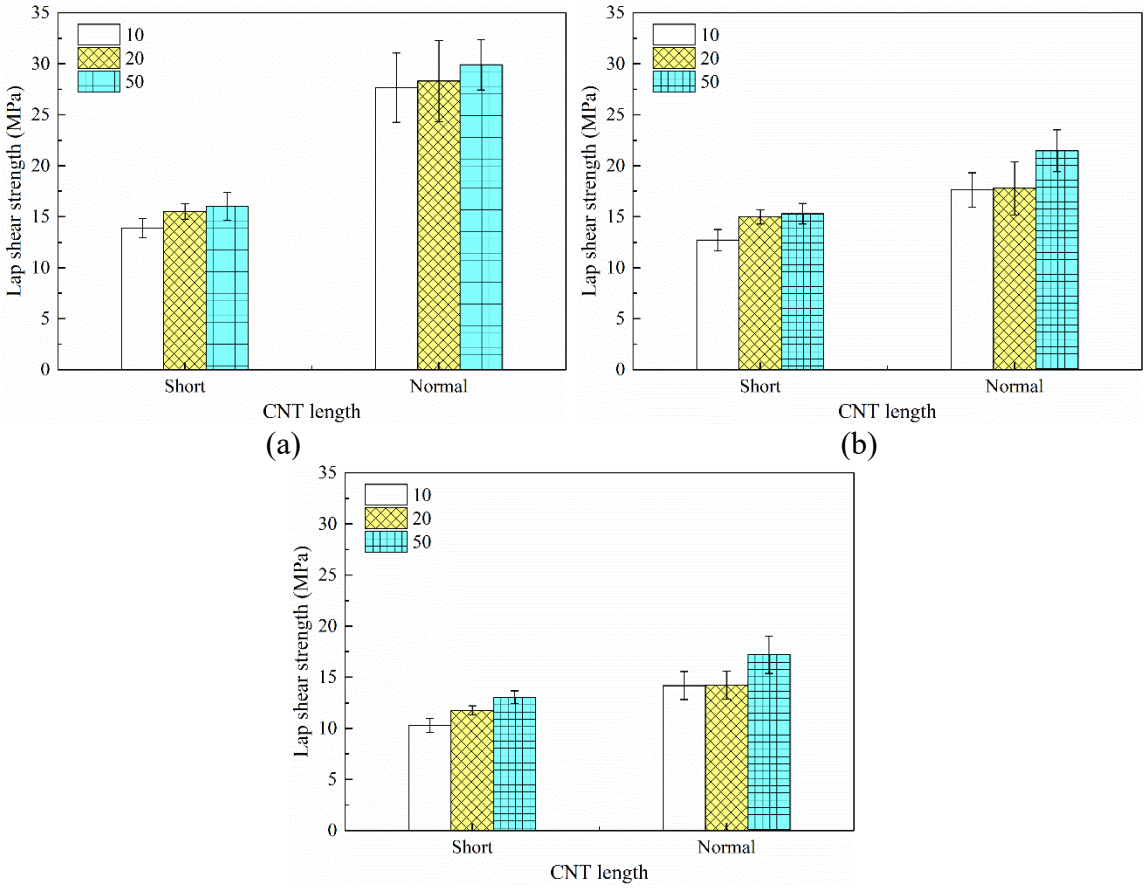

611 Fig. 8 Lap shear strenths of CNT reinforced epoxy composites with different CNT
612 geometries: (a) 0.5%; (b) 1%; (c) 2% CNT fractions.

613

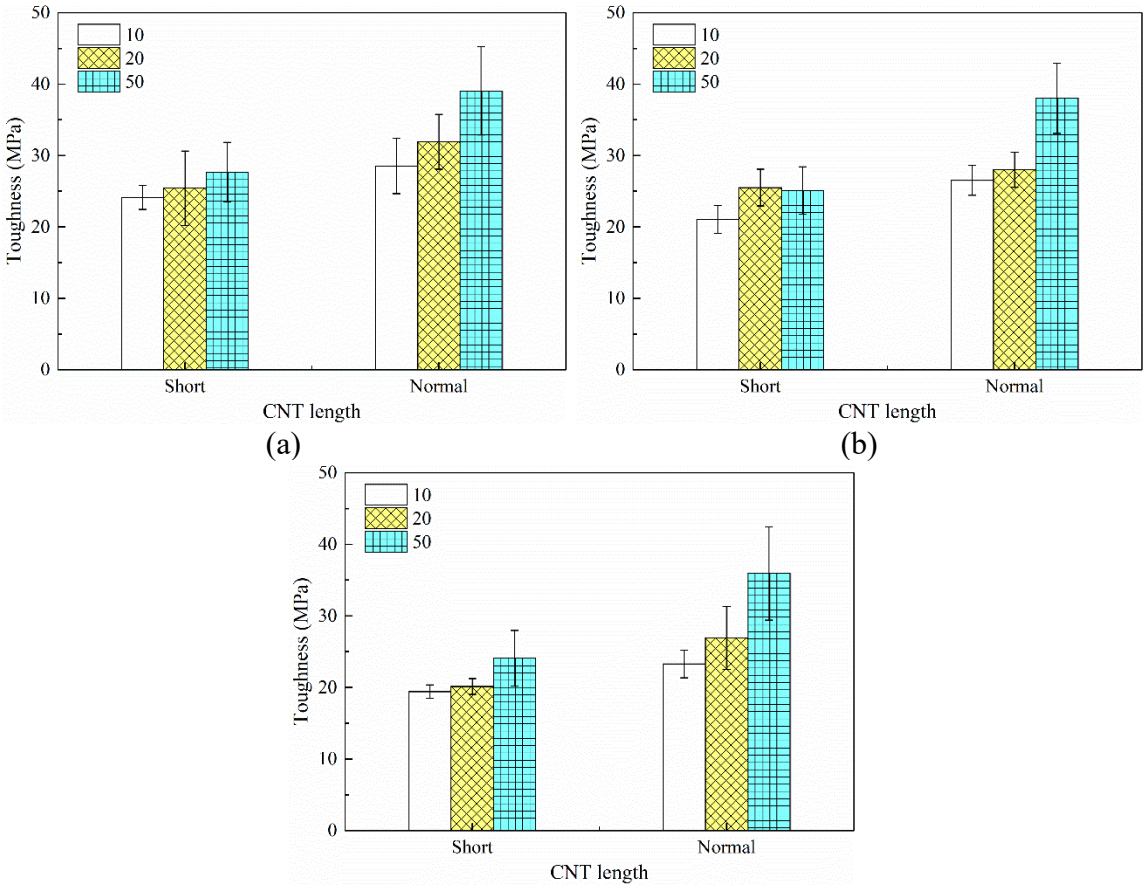

614 Fig. 9 Toughness of CNT reinforced epoxy composites with different CNT geometries:
615 (a) 0.5%; (b) 1%; (c) 2% CNT fractions.

616

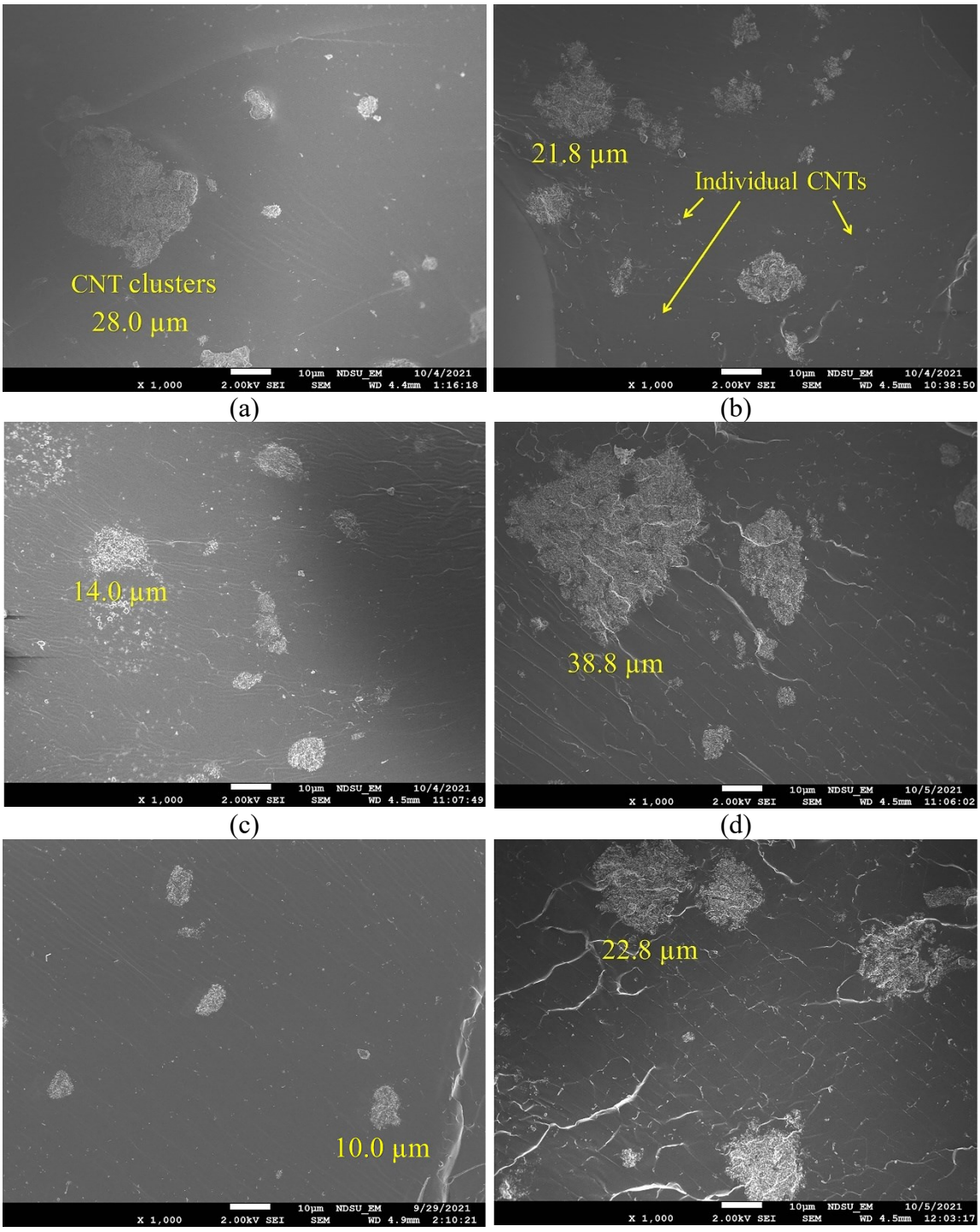

Fig. 10 SEM images on the fracutre surfaces of CNT reinforced epoxy composites: (a) N10-0.5; (b) N20-1; (c) N20-0.5; (d) N20-2; (e) N50-0.5; (f) S50-0.5.

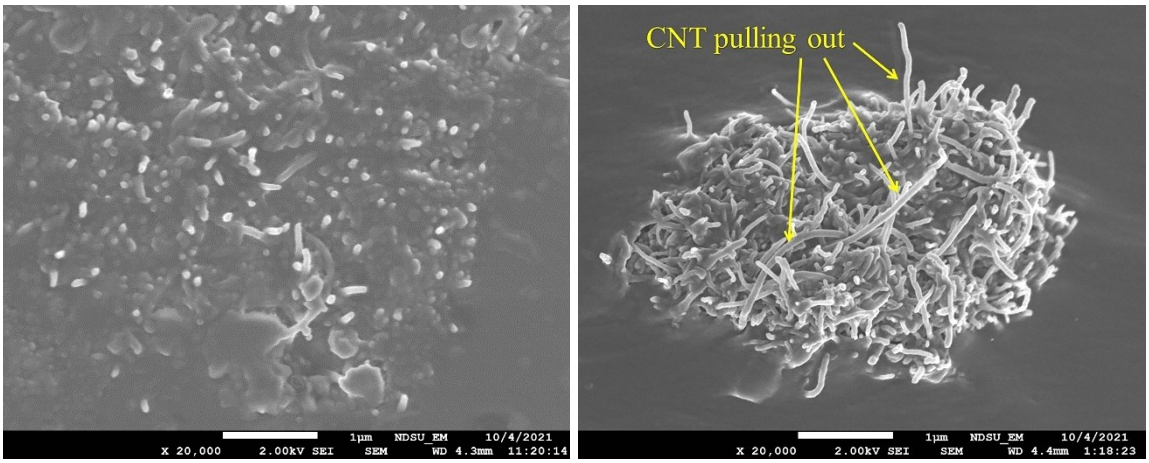

(a) (b)

620 Fig. 11 SEM images at high magnification: (a) N10-0.5; (b) N50-0.5